Available online at www.sciencedirect.com
ScienceDirect
C. R. Physique 10 (2009) 176–187
COMPTES RENDUS PHYSIQUE

Laser acceleration of particles in plasmas / Accélération laser de particules dans les plasmas

Laser acceleration of low emittance, high energy ions and applications

Julien Fuchs [a,*], Patrick Audebert [a], Marco Borghesi [b], Henri Pépin [c], Oswald Willi [d]

[a] *LULI, École polytechnique, CNRS, CEA, UPMC, route de Saclay, 91128 Palaiseau, France*
[b] *School of Mathematics and Physics, The Queen's University, Belfast, United Kingdom*
[c] *INRS-EMT, Varennes, Québec, Canada*
[d] *Institut für Laser und Plasma Physik, Heinrich-Heine-Universität Düsseldorf, Universitätstrasse 1, 40225 Düsseldorf, Germany*

Available online 5 May 2009

Abstract

Laser-accelerated ion sources have exceptional properties, i.e. high brightness and high spectral cut-off (56 MeV at present), high directionality and laminarity (at least 100-fold better than conventional accelerators beams), short burst duration (ps). Thanks to these properties, these sources open new opportunities for applications. Among these, we have already explored their use for proton radiography of fields in plasmas and for warm dense matter generation. These sources could also stimulate development of compact ion accelerators or be used for medical applications. To extend the range of applications, ion energy and conversion efficiency must however be increased. Two strategies for doing so using present-day lasers have been successfully explored in LULI experiments. In view of applications, it is also essential to control (i.e. collimate and energy select) these beams. For this purpose, we have developed an ultra-fast laser-triggered micro-lens providing tuneable control of the beam divergence as well as energy selection. ***To cite this article: J. Fuchs et al., C. R. Physique 10 (2009).***

Résumé

Accélération laser d'ions énergétiques de faible émittance et applications. Les sources d'ions accélérées par laser de forte puissance possèdent des propriétés exceptionnelles, c'est-à-dire une forte luminosité et une forte énergie (56 MeV à l'heure actuelle), elles sont aussi directionnelles et extrêmement laminaires (au moins 100 fois plus que les sources produites par les accélérateurs conventionnels) et ont une très courte durée d'impulsion à la source (ps). De par ces propriétés, ces sources ouvrent de nouvelles possibilités pour les applications des faisceaux d'ions. Parmi celles-ci, nous avons déjà exploré l'utilisation de la radiographie de protons à la physique des plasmas et pour la production de matière dense et chaude. Ces sources pourraient également stimuler le développement d'accélérateurs d'ions compact ou pourraient être utilisées pour des applications médicales. Pour étendre la gamme des applications potentielles, l'énergie des ions ainsi que l'efficacité de conversion laser/ions doit cependant être augmentée. Deux stratégies pour y parvenir en utilisant les lasers actuellement disponibles ont été explorées avec succès dans des expériences réalisées au LULI. Il est également essentiel de contrôler les caractéristiques de ces faisceaux. À cette fin, nous avons développé une micro-lentille plasma déclenchée par laser ultra-rapide et accordable afin de contrôler la divergence du faisceau ainsi que de le sélectionner en énergie. ***Pour citer cet article : J. Fuchs et al., C. R. Physique 10 (2009).***

Keywords: High-power laser; Ion beam; Low-emittance beam; High-current beams; Proton radiography; Warm dense matter

* Corresponding author.
E-mail address: julien@greco2.polytechnique.fr (J. Fuchs).

1631-0705/$ – see front matter
doi:10.1016/j.crhy.2009.03.011

Mots-clés : Laser de puissance ; Faisceau d'ions ; Faisceau de faible émittance ; Radiographie de protons ; Matière dense et tiède

1. Introduction

The observation of ultra-intense laser-accelerated ion beams [1] represents one of the most exciting developments of "strong field science". Indeed, the beams have unique properties, namely their high current, their short duration (ps), their extremely good laminarity [2,3], the high number of protons (10^{11}–10^{13} ions in a single bunch) that can be produced, as well as the possibility to tailor their spectrum [4–6] and their beam divergence [6,7]. Moreover, these sources are extremely compact (the acceleration occurs over a distance of about tens of microns). All this, coupled to the fact that they are naturally synchronized with laser beams, offer original prospects as tools to explore fundamental properties of matter. High-power laser produced energetic proton beams are already applied for high-resolution charged-particle radiography [8] or to produce warm-dense matter [7]. Further proposed applications include the use of laser-driven proton beams to ignite [9] pre-compressed capsules in the "Fast Ignitor" (FI) [10] scenario of inertial confinement fusion using future multikilojoule petawatt laser facilities [11], or as high-brightness injectors for accelerators [3], sources for proton therapy [12–14] or radioisotope production [15].

Such beams have been only recently observed since they require extremely high laser intensities that have been made available in recent years (the first observations were independently published in 2000 by three research groups [16–18]) thanks to the fast progress of short-pulse laser technology [19]. In the following, we will review recent progress in this area that has been achieved in experiments performed at the LULI laboratory, including results obtained very recently.

2. Experimental requirements

All the results that will be discussed here have been obtained in experiments performed using the LULI 100 TW laser facility working in the chirped pulse amplification (CPA) regime [19]. This facility has a main compressed CPA laser beam working at a wavelength of $\lambda_0 = 1.056$ μm, having 20 J of laser energy and a pulse duration of 320 fs. As standard with such lasers, this short pulse is preceded by a 500-ps long pedestal at $\sim 10^{12}$ W/cm^2. The laser is focused to a FWHM of ∼6 μm with a good repeatability since wave front correction is applied before every shot. This allows to reach peak intensities at focus of about $3\text{–}5\times 10^{19}$ W/cm^2. The facility has also the capability of a second independently compressed laser pulse, of lower energy (10 J) that is used for auxiliary purposes (see below Sections 5.4 and 7.1).

The proton energy spectrum is usually measured with magnetic ion spectrometers [20] and Thomson parabolas. The transverse beam profile is measured using dosimetric film (RCF) packs [21]. RCF are preferentially sensitive to penetrating protons, which have a large specific energy-loss and produce a high contrast image.

3. Mechanisms

As illustrated in Fig. 1, the high-current, collimated multi-MeV beams of protons are generated by irradiating thin solid foils with ultra-intense ($>10^{18}$ W cm^{-2}) short-pulse lasers (30 fs–10 ps). Several mechanisms have been observed, in experiments or simulations, to induce proton and ion acceleration, namely Target Normal Sheath Acceleration (TNSA) [22], front-surface acceleration [23], and shock acceleration [24]. However, the TNSA mechanism is the one, up to the presently accessible highest laser intensities, that has produced (i) the highest energy ions and (ii) the most laminar beam. When using solid targets, TNSA accelerates high energy protons normal to the target surfaces. For standard laser temporal contrast conditions (i.e. when a pedestal precedes the main laser pulse), only the initially cold non-irradiated (rear) surface produces a good quality beam, propagating in the forward direction (i.e. away from the laser) [25] (see Section 5.3) because only this surface has a sharp interface with vacuum [25–27]. Laminar acceleration in the backward direction (toward the laser), of ions generated at the target front surface, is also possible but it requires very high-contrast laser pulses [28]. TNSA proceeds as follows: at the rear target–vacuum interface, relativistic electrons laser-accelerated from the front side into the target form a dense electron plasma sheath. At the laser-intensities considered here, MeV electrons have a mean-free path that is much larger than the typical target thickness (a few tens of microns). Therefore, the electrons can cross the target material and exit into vacuum.

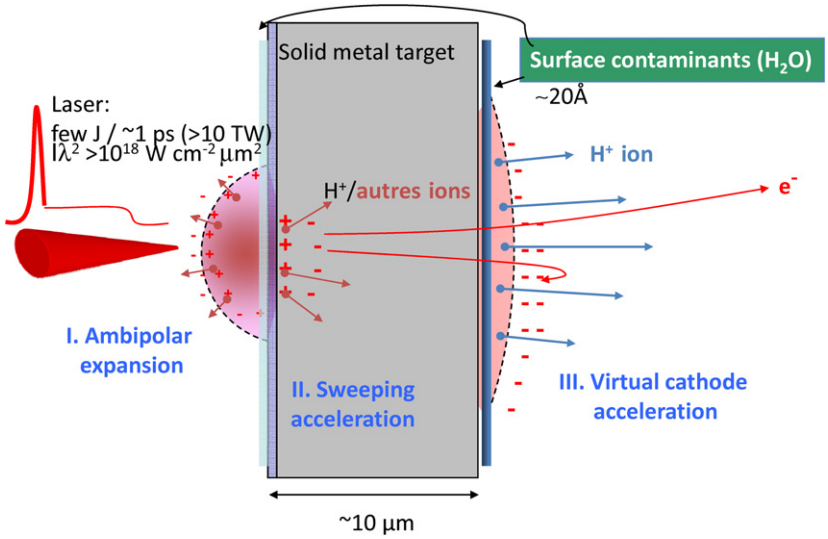

Fig. 1. Schematic of the various mechanisms leading to laser-acceleration of high-energy ions by a short, high-intensity laser pulse irradiating a thin target.

Most of the electrons are however retained at the target surface due to the potential that has built within the target. The charge-separation field that results from the formation of the sheath on the rear surface of the target is initially of the order of $\phi_{\text{ponderomotive}}/(e\lambda_D)$ where $\lambda_D \sim 1$ µm is the Debye length in the solid target for MeV electrons. This field, being of the order of a few TV/m, ionizes the surface atoms almost instantaneously and rapidly accelerates ions in the direction normal to the initially unperturbed surface [22].

It was seen in the first experiments that protons were accelerated using metal foils, such as Au or Al. The independence from target material suggested that the main ion signal comes from protons contained in a surface layer of water vapor and hydrocarbon contaminants [29,26]. This layer, typically 20 Å thick, is usually present on targets under normal preparation and handling conditions. Hydrogen atoms, having the lowest q/m ratio, will be preferentially accelerated. If heating of the target is performed prior to the experiments in order to eliminate the hydrogen contaminants as much as possible, the acceleration of heavier ions is favored [4]. By simply changing the substrate, laser-acceleration can therefore produce a versatile, easy to modify source of ions.

Together with the electrons that were part of the initial sheath, the accelerated ions expand in vacuum. As the laser is switched off, the electrons cool down by adiabatic energy transfer to the ions [30], leading to a decrease of the driving electric field [31]. The electrons eventually drift at the same velocity as the ions and the ion energy saturates, leading to a sharp high-energy cut-off [30], as observed in all experiments [1]. With the peak intensity available at LULI (about $3\text{–}5 \times 10^{19}$ W/cm^2), protons are accelerated up to 20–30 MeV energies from thin metallic target (e.g. Al or Au foils with thickness of a few tens of microns). Experiments using lasers with energies as low as few hundreds of mJ have also reported accelerated protons, also of lower kinetic energies (a few hundreds of keV). The present record in terms of kinetic energy has been set by the Nova PW laser facility at LLNL which has produced up to 56 MeV protons [17].

4. Electron sheath density measurement

The parameters of the electron sheath (density, spatial distribution) are crucial in determining the ion acceleration process. For example, the lateral extension of the electron sheath governs the zone over which ions are accelerated. This lateral extension depends mainly on the divergence of the hot electrons as they enter the solid as the electron source at the front has dimensions of the order of the laser focal spot. Indirect measurements and simulations suggested that the electrons diverge with $>25°$ half-angle [32–34], but this lacked a precise determination. It was also debated whether the electron sheath was bell-shaped or parabolically-shaped [32,35,36]. In order to obtain a better knowledge of the hot electrons sheath characteristics, we have recently measured the parameters of the accelerating sheath. In particular, we have shown that the density of the hot electrons on the target rear surface is bell-shaped, with a half-

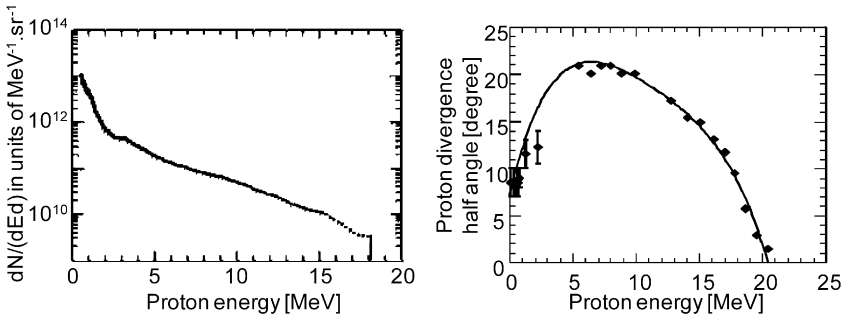

Fig. 2. (left) Typical spectrum of protons laser-accelerated from a 10 μm thick Au foil irradiated by a 3×10^{19} W cm^{-2}, 350 fs laser pulse, as measured by a magnetic spectrometer. (right) Variation of the proton divergence half angle vs. the proton energy using the same laser and target parameters.

maximum radius ∼100 μm for a 10 μm thick target, and that the mean fast electron energy at the same location is radially homogeneous and decreases with the target thickness [37].

5. Beam characteristics

The high energy proton beams accelerated by the TNSA mechanism detailed above (see Section 3) have fundamentally different properties from lower energy protons observed in earlier work conducted at lower laser intensity with laser pulses in the nanosecond and tens of picosecond regime [29].

5.1. Energy and particle number

Contrary to the early experiments performed in the 1970s, beams accelerated by ultra-intense laser pulses exhibit a high number of ions per bunch (spread however over a large spectrum, see Fig. 2), a limited divergence (the beam is emitted in a well-defined cone), an extreme laminarity, and a high cut-off energy in the 10–30 MeV range for our parameters. The emission is along the normal to the un-irradiated rear surface of the target. Note that we have fully characterized the proton beam even at low energies, i.e. below 1 MeV, as this part of the spectrum plays an important role in isochoric heating of matter (see Section 7.2).

A review of the maximum energy and proton number obtained in various experiments is shown in Fig. 3. Fig. 3(left) shows the evolution of the recorded maximum proton energy as a function of the pulse duration. The data have been grouped so that similar conditions (e.g. similar laser intensities) in experiments carried out in different laboratories could be compared. This figure shows clearly that the maximum proton energy increases with the laser pulse duration, the increase following roughly parallel lines for varying laser irradiances. The lines overlaid on the plot for various laser intensities represent the scaling given by a simple model which has been confronted to a systematic series of experiments [38]. Fig. 3(right) shows that not only the maximum proton energy but also the efficiency of the acceleration process increases with the laser pulse duration and the laser irradiance.

5.2. Angular characteristics

Since the ions are accelerated by the electron sheath, their spatial and angular characteristics are determined by the electron density distribution within the sheath. At high energy, the proton beam exhibits an angular distribution with a sharp boundary. As was discussed in Section 4, the electron sheath follows a generic bell-shaped spatial distribution. Having this in mind, both the existence of a sharp angular boundary in the proton angular distribution and the decrease of the beam divergence with energy are easily understood. Indeed, the higher energy protons are accelerated from the tip of the sheath with a very small divergence angle. The acceleration of lower energy protons takes place from larger regions including the wings of the sheath. As the ions are accelerated normal to the electron density iso-contours, ions of lower energy will therefore have larger divergence than the ones accelerated from the sheath tip. This is clearly observed experimentally [17].

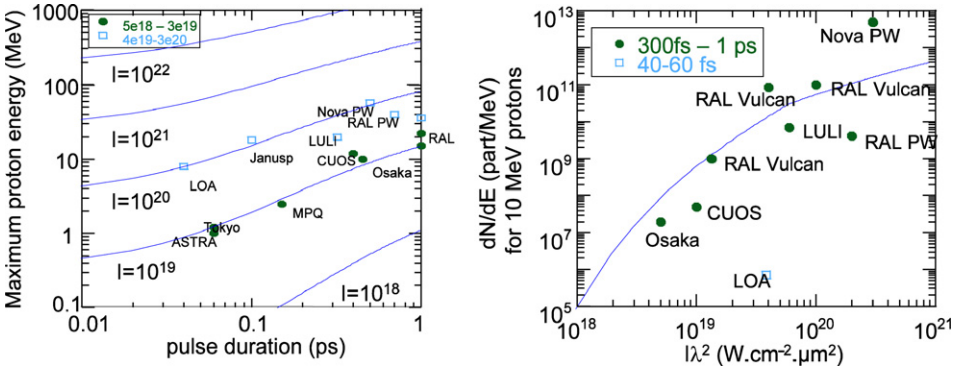

Fig. 3. Review of (left) cut-off maximum proton beam energy and (right) number of protons in a 1 MeV bin around 10 MeV as reported from published data. The left plot is as a function of laser pulse duration. Dots and squares are experimental data for the two intensity ranges shown in the legend box, the intensities are in units of W cm^{-2}. Lines represent calculations following the model detailed in Ref. [38] for various laser intensities, as indicated in units of W cm^{-2}, assuming 20 μm thick targets and a 10 μm FWHM laser spot size. The right plot is shown as a function of laser intensity multiplied by the laser wavelength square. The last parameter is chosen since it governs the hot electron temperature. Dots and squares are experimental data for the two laser pulse duration ranges shown in the legend box. The line is still given by the same model assuming 20 μm thick targets, a 10 μm FWHM laser spot size and a 0.5 ps duration laser pulse.

The measurement of the electron sheath characteristics discussed in Section 4 was obtained in the peculiar case of polished thin metal targets and using a smooth laser focal spot. If one deviates from these ideal conditions, the proton angular distribution will be perturbed. Deviations can arise from the target surface roughness, the target shape, and the laser focal distribution. We have indeed experimentally observed that using an insulator target, a roughened target surface, or a modulated laser focal spot will produce an unsmooth proton beam [39].

5.3. Laminarity and emittance

A unique and most interesting characteristic of the laser-accelerated proton beam lies in its high degree of laminarity [3], or equivalently its extremely small apparent source size [2]. This is the key factor that enables applications such as high-spatial resolution radiography, and that makes these sources potentially interesting as high-brightness injectors for accelerators. Laminarity is most precisely measured by producing fiducials of the beam flow. Such fiducials are produced by purposefully micro-machining shallow grooves on the target surface [3,40]. Using this technique, it is possible to image the proton-emitting surface, to reconstruct the transverse phase-space of the beam flow, and to determine the transverse emittance. In particular, we have shown that the root-mean-square (rms) value of the normalized emittance ε_N is, for protons of up to 10 MeV, as low as 0.0025 mm mrad, i.e. 100-fold better than typical RF accelerators and at a substantially higher ion current (kA range). It is important to note that this value is actually an upper limit that is limited by the experimental technique and that the real emittance could be even lower.

We have also shown [3] that the removal of the co-moving electrons, as required e.g. to capture the ions into a post-accelerator, after 1 cm of the quasi-neutral (protons and electrons) beam expansion did not increase significantly the measured proton transverse emittance.

The exceptionally low emittance stems from the extremely strong, transient acceleration that takes place from a cold, initially unperturbed surface and from the fact that during much of the acceleration the proton space charge is neutralized by the co-moving hot electrons.

5.4. Beam handling

An important requirement for many applications is the ability (i) to refocus the beam on a target or to collimate it in order to transport it over large distances, and (ii) to select a sufficiently small energy spread $\Delta E/E \ll 1$ out of the energy spectrum of the beam.

Compared to other solutions that have been explored [7,41,4,5] which involved complex target engineering or prevented the possibility of using the whole beam [42], we have developed an ultrafast laser-triggered micro-lens [6]

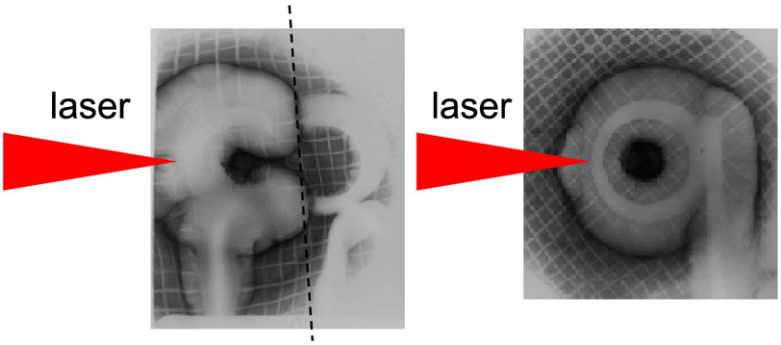

Fig. 4. (left) RCF showing the angular distribution of 6 MeV protons that have transited longitudinally through a cylinder (diameter 800 μm, length 470 μm) cut in two halves (the dashed line indicates the separation axis) irradiated by a 3×10^{18} W cm^{-2}, 320 fs laser. These protons are accelerated by a 5×10^{19} W cm^{-2}, 320 fs laser. (right) Same with the full cylinder.

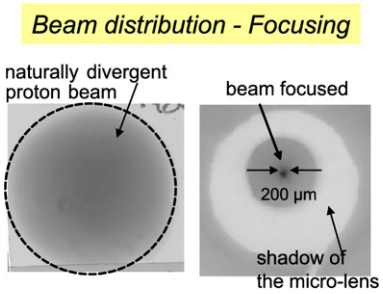

Fig. 5. Effect of the micro-lens on the angular distribution of the proton beam. A small fraction of the energy spectrum (from 6 MeV to 6.3 MeV) is focused into a 200 μm spot.

that allows to solve simultaneously the two issues mentioned above. This device provides tuneable, simultaneous focusing and energy selection of MeV proton beams, while also withstanding large ion beam currents. The principle of operation is rather simple: A diverging proton beam produced at the rear of a laser irradiated thin foil target is directed onto a hollow, thin-wall cylinder typically 1 mm in diameter. This hollow cylinder is irradiated by an auxiliary laser pulse. This pulse injects relativistic electrons through the cylinder's wall. These electrons spread evenly on the cylinder's inner walls and initiate hot plasma expansion. The radially symmetric, transient electron fields associated to the expansion can act to focus a fraction of the proton beam along the axis of the cylinder (the fraction that transits at the time the device is switched).

Homogeneous electron spread around the cylinder is experimentally demonstrated as shown in Fig. 4. Here we use proton radiography of the fields associated with the Debye sheath generated by the hot electrons. We clearly observe that in the case the cylinder is cut in two halves, see Fig. 4(left), no electron sheath is induced on the wall surface opposite to the irradiation point. This shows that the electrons, accelerated at the interaction point, reach the opposite side of the cylinder by spreading along its surface and not by crossing the vacuum gap at the center of the cylinder. When a full cylinder was used, see Fig. 4(right), we can observe that the fields are symmetric around the cylinder, demonstrating a symmetric electrons spread.

The focusing due to the transient electric fields can be seen in Fig. 4(right) by the inner contraction of the probe proton beam transiting along the cylinder's axis. In this case, the focusing is not very strong due to the short length of the cylinder (470 μm). If we use a longer cylinder (e.g. 3 mm), the range over which the on-axis probing protons sense the focusing sheath electric fields is increased. This results in a tight focusing capability, as shown in Fig. 5. Note that since the electric field produced in the cylinder is intrinsically transient, only the protons propagating through the cylinder near the peak of the irradiating laser pulse will be focused. Thanks to this effect, the device can selectively focus protons within a particular energy range out of the beam's broad spectrum (due to energy dependence of the source-to-cylinder time-of-flight).

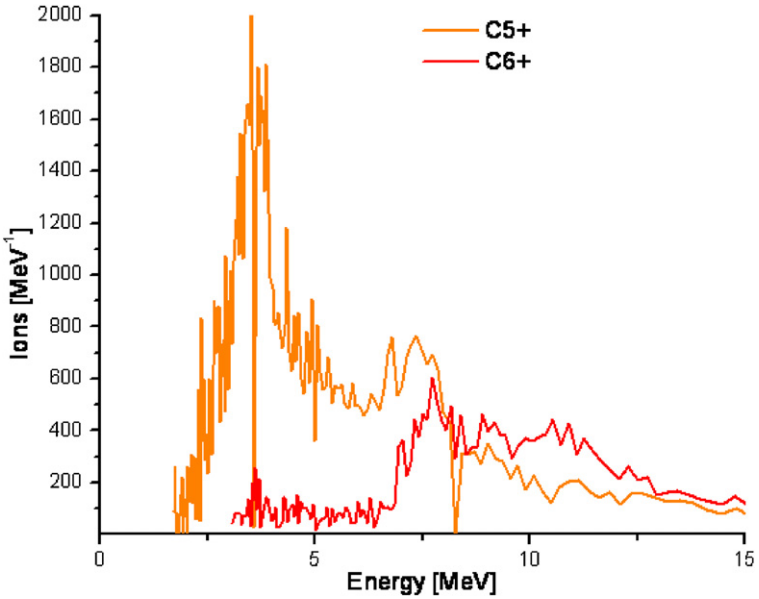

Fig. 6. Carbon spectra of beams accelerated by a 5×10^{19} W cm^{-2}, 320 fs laser irradiating a 20 μm thick C heated target and passing through a laser-triggered micro-lens.

This device also allows simultaneously for tuneable energy selection of the energy spectrum by positioning appropriate apertures downstream in the beam [6]. The tuneability is obtained by varying the time at which the micro-lens is triggered compared when the protons transit through it.

The micro-lens has also the ability to focus ion beams and not only protons. To demonstrate this, we generated a beam of C ions. This beam was obtained, as mentioned in Section 5, by heating, using an auxiliary CW (5 W) laser, carbon targets to remove the hydrogen-rich surface contaminants. A shown in Fig. 6 by the spectral peaks obtained for different charge states of C after passing through the laser-triggered cylinder, we could indeed energy select charged carbon beams.

6. Optimization of the proton beams properties

Beam optimization of laser-accelerated protons is a crucial point for the development of applications in various areas. Several directions need to be pursued: (i) optimization of the high-energy end of the spectrum e.g. for dense plasma radiography; (ii) optimization of the low-energy end of the spectrum e.g. for isochoric heating of matter; (iii) enhancement of laser-to-protons conversion efficiency and reduction of divergence e.g. for fast ignition.

As shown in Fig. 7, simply scaling the presently known TNSA mechanism to higher laser intensity shows that several hundred MeV protons could be achievable with foreseeable future high-power lasers [38], e.g. the future ELI facility (the expected intensities at various stages of its development are also indicated in Fig. 7).

Simulations performed at higher laser intensities than presently achievable suggest that other mechanisms than the currently explored ones could accelerate ions at high energy. For example, ions could be shock accelerated at the target front surface or in its interior [24]. Simulations indicate that for laser pulses with intensities roughly $I > 10^{21}$ W cm^{-2}, shock-accelerated protons could be more energetic than the ones accelerated by TNSA. At even higher laser intensities (up to $\sim 10^{23}$ W cm^{-2}), the transition to another extreme ion acceleration regime is predicted [43]. In this mechanism, the radiation pressure of the electromagnetic wave is directly converted into ion energy via the space-charge force related to the displacement of the electrons in a thin foil, allowing to reach GeV-scale energies.

Besides relying on the expected intensity increase of future laser facilities, other routes can be explored in order to optimize, in the context of TNSA acceleration, either the laser generation of hot electrons and/or the way these electrons are distributed to the target–vacuum interface where the ions are accelerated. Some possible approaches are discussed in the following sections.

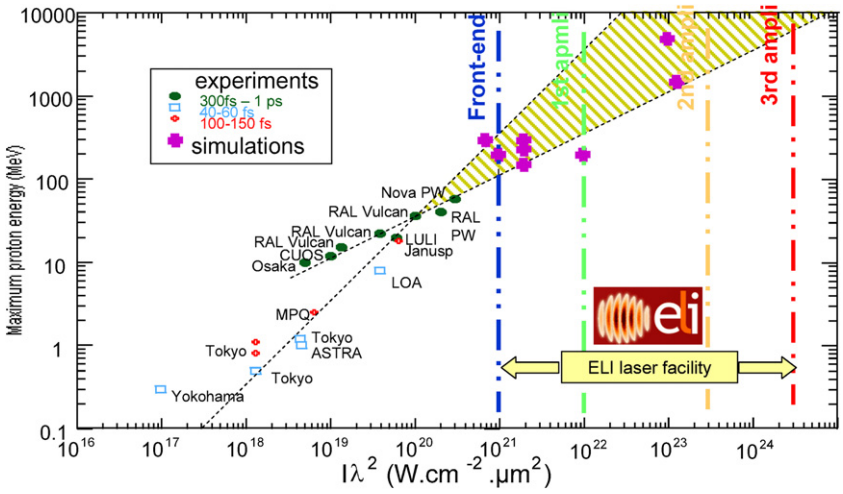

Fig. 7. Review of cut-off maximum proton beam energy, as a function of laser intensity, as reported from published data. Experimentally measured data are small dots, boxes and crosses corresponding to three pulse duration ranges shown. Simulations performed at higher laser intensities than presently accessible are reported as big purple dots.

6.1. *Proton acceleration from ultra-thin targets*

An approach is to use ultra-thin targets (say 30–100 nm) in which the laser absorption is increased as compared to thicker targets used in the standard acceleration regime. In LULI experiments, these ultra-thin targets were irradiated with laser pulses of 320 fs duration, 1 J energy and 10^{18} W cm^{-2} μm^2 intensity. In order for the laser to interact with ultra-thin targets, the contrast ratio of the laser pulse ahead of the main laser pulse (i.e. the ratio between the intensity in the pedestal preceding the main pulse and the peak intensity of the main pulse) needs to be very high otherwise the laser pedestal destroys the target before the main pulse irradiates it. In order to enhance the contrast ratio, we have used plasma mirrors [44] although at the cost of a reduction of the on-target laser energy. The plasma mirror consists of an anti-reflection-coated optically polished glass slab, so that most of the undesired pedestal energy is transmitted while the energetic main laser pulse reflects on a plasma created at the mirror surface. It was then possible to accelerate proton beams to a maximum energy of ∼7.3 MeV from targets as thin as 30 nm thick [44], which represents an increase in energy of at least a factor 8 compared to the acceleration from thicker targets, i.e. 5 μm thick, using the same intensity. To obtain similar proton energy, 20 times higher laser intensity, i.e. 2×10^{19} W cm^{-2} μm^2, is required using thicker (25 μm) target. Comparing similar achieved proton energies, the laser to proton energy conversion is also increased, from typical values of 0.1% to 4% [45]. 2D PIC simulations, which were in close agreement with the results, suggest more efficient laser absorption and electron heating as compared to thicker targets. The 2D simulations show the potential of laser-acceleration of protons from ultra-thin targets using ultra-high contrast pulses. Proton energies of 50 MeV should be obtained from 50 nm targets with an intensity of 3×10^{19} W/cm^2, and a pulse duration of 350 fs.

Using ultra-thin targets is therefore a way to efficiently increase the energy of laser-accelerated protons as compared to the standard regime of acceleration using thick foils. This should orient development of future lasers as, to fully exploit this regime, they should be conceived natively with high temporal contrast to avoid losing laser energy when *cleaning* the pulse with e.g. plasma mirrors.

6.2. *Proton acceleration from reduced-mass targets*

Another approach is to enhance the laser-acceleration of protons from solids by increasing the initial density of the electrons that are at the source of the ion acceleration. The measurements of the sheath extension that were presented in Section 4 show that, on solid foils of extended lateral dimensions (∼mm), the accelerating sheath extends over a relatively large area (typically ∼100–200 μm in radius) at the rear of the target. By limiting the transverse size of the target below this size, while maintaining its thickness sufficiently small, we tested whether it would be possible to increase significantly the accelerating field, as underlined recently in theoretical work [46]. In order to reduce the

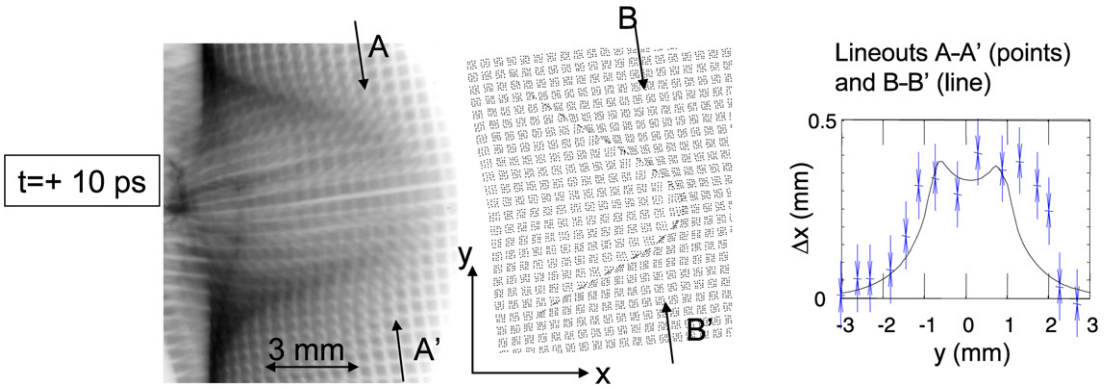

Fig. 8. Proton probing of electric fields generated by the ultra-fast charge-dynamics following the production of relativistic electrons by an intense laser. The proton deflectometry data on the left [31] shows the expanding plasma front into vacuum driven by the hot electrons. The image is taken 10 ps after the expansion is initiated. The image in the middle is a post-processing of a plasma expansion simulation using the same parameters in the experiments. The plot on the right, presenting lineouts of the data (points) and of the simulation (solid line), shows that there is a good quantitative agreement between the experimental image and the simulation post-processing as the observed proton deflection is well reproduced.

contrast and avoid preplasma leaking from the front to the rear surface, we used frequency doubling of the laser. Although this caused a reduction in irradiance, we were able to employ foils as thin as 2 μm and down to 50–80 μm width. In the experiment, a very significant energy increase was observed, doubling the peak proton energy when using the smallest targets compared to large targets (mm lateral size). We simultaneously observed that smaller targets presented a much higher proton flux, and also an increase in beam collimation. Simultaneously, the conversion efficiency from lasers to ions grows by 3 orders of magnitudes by moving to the smallest targets [47]. The observed dose is very promising for applications such as proton-isochoric heating of matter, or for radioisotope generation, where the laser-to-proton yield is the appropriate figure of merit.

7. Applications

In this section, we will discuss briefly two applications of laser-accelerated proton beams that we pursued: (i) their use as a probe for the measurement of transient electric fields; and (ii) for the production of warm dense matter.

7.1. Proton probing of electric fields

Proton beams are a powerful tool for investigating highly transient electric and magnetic fields. A technique that allows one to obtain quantitative information on these fields is proton imaging/deflectometry, which detects electric and magnetic fields via the deflection induced on the protons of a particle probe. The deflected beams are collected on stacks of RCF, providing directly 2D transverse imaging of the deflection patterns and hence enable the reconstruction of the field distribution. As different proton energies correspond to different layers of RCF in the stack, we also obtain directly, imprinted in the various RCF layers, the fields' temporal evolution. This is due to the time of flight difference for the different proton energies between the proton source and the probed field zone. Due to the excellent laminarity of the beams, the spatial resolution is of the order of a few μm. Due to the intrinsically short acceleration time, the temporal resolution (limited by the energy range integrated in each RCF layer and by the proton transit time in the field region) is of the order of a few ps.

An example of the use of this technique in detecting electric fields is shown in Fig. 8. Here we aimed at measuring the electric fields responsible for the acceleration of high-energy protons from a solid thin foil irradiated by an intense short pulse laser, i.e. fields that are relatively well known theoretically from adiabatic plasma expansion models. The experiment used the two intense short pulses of the LULI 100 TW, focused at close to 90° from each other. The two proton beams generated by the irradiation of the two beams on solid targets were detected in multiple layers of RCF. Beam 1 (the proton-probe generating beam) was delayed with respect to beam 2 so that the proton accelerating phase on the rear-surface of target 2 could be probed.

The electric field structure associated with the plasma expanding from target 2 irradiated by beam 2 can be seen in Fig. 8. To obtain quantitative information on the deflections and on the electric field spatial distribution, we have inserted a fine copper mesh in between target 1 and target 2, so that a regular pattern is imposed on the proton probe beam [2]. After crossing target 2, the mesh is observed to be locally deformed due to the electric fields deflecting the probing protons. The deformations are bell-shaped, reminding the shape of the sheath observed in the experiment mentioned in Section 4, with a clear jump at the mesh edge and a regular grid structure within the distorted zone. The tip of the deformation is observed to expand outwards as time increase. Using the deformations of the regular mesh we can estimate E-fields values at the front of the expansion. We measure at the ion front a deformation of the grid of $\Delta x \sim 0.3$ mm, which can be linked to the field knowing that the transverse momentum given to the proton by the electric field is $m_e v_\perp = eE_\perp \tau$. Here τ is the crossing time in the field, i.e. $\tau \sim \Phi/v_{//}$ where $v_{//}$ is the proton longitudinal velocity and Φ is the lateral dimension of the field structure expanding from target 2. This is estimated from the film as $\sim$60 μm. We have therefore $\Delta x = (v_\perp/v_{//})d = deE_\perp \Phi/(m_p v_{//}^2)$, d being the distance between target 2 and the film (2.8 cm). Thus, we can infer a value $E_\perp \sim 3 \times 10^9$ V/m.

This value meets the one predicted at the same time by a relativistic adiabatic expansion code [30] using the same parameters as in the experiment. Beyond the value of the field at the tip of the expansion, the whole electric field structure observed in the experiment is in very good agreement with the simulations, as can be seen in Fig. 8. For this, we use the electric field profiles given by the simulation of a collisionless expansion of a thin foil into a vacuum, then post-processing them to calculate the trajectories of the probing protons up to the RCF layer on which they are collected. Most notably, this shows that the predicted peaked structure of the accelerating field at the expanding ion front [30] is observed.

7.2. Production of warm dense matter states

Producing, in a controlled way, media at high temperature (10–25 eV) while maintaining them at high density (a few g/cm^3) is of prime interest; it would allow studying matter under conditions relevant to a number of research areas, from fundamental plasma physics to classical inertial confinement fusion or fast ignition. Such a warm and dense state can be achieved in laser-irradiated samples but, due to the skin-depth penetration of visible or IR light in solids, only in volumes too small to allow an accurate characterization. Some experiments carried out recently [7,48] have shown the usefulness of laser-accelerated proton beams since they deposit their energy volumetrically (the so-called "Bragg peak"). Furthermore, they are produced in a very short bunch (less than 1 ps when exiting the source) and thus can heat samples before they start to expand.

The experiment is rather straight-forward: a first target (the proton source) is positioned at the focus of a high-intensity laser, producing a laminar proton beam with a maximum energy of 20 MeV as has been detailed above. This proton beam irradiates and heats a secondary solid target positioned after a vacuum gap (200 μm in our experiments), where the protons stop and deposit their energy. In order to characterize the sample temperature, we first characterized the proton source, in particular the low-energy ($\sim$1 MeV, see Section 6.1) part that induces most of the heating. Next, this source is used in a heating model, namely the one-dimensional code (1D) hydrodynamic Esther [49] in which proton stopping models are implemented. Note that the simulations use the independently measured proton energy distribution, i.e. *there are no free parameters in the simulations*. The output of the code needs then to be confronted with data obtained with the heating experimental diagnostics. We found that the most reliable diagnostic was via the measurement of the proton heated target rear-surface expansion speed, similar to what mentioned in Section 4 but this time not measuring the expansion of the hot electron cloud but that of the colder target bulk. Simulations show that the target is heated in a few picoseconds to temperatures of a few eV.

Fig. 9 shows, for the same target, the comparison between the simulated phase and the experimental phase for the target expansion diagnostic. The plot shows the phase of the probe beam after reflection off the target as a function of time (each curve is obtained in a single shot). The phase decreases with time due to target expansion. In Fig. 9, three experimental probe beam phases are plotted, resulting from measured shot-to-shot fluctuations of the incident proton beam irradiating the target. The simulations have also been performed for the various proton spectra we could record (although on separate shots). These give the shaded area showing the range of probe beam phases simulated in the code. There are two shaded areas as the code has been run using two equations of state, one where the target material is described by a multiphase equation of state spanning a large range of density and temperature from hot plasma to cold condensed matter (BLF) and one using the SESAME table. Fig. 9 shows that, in spite of the recorded

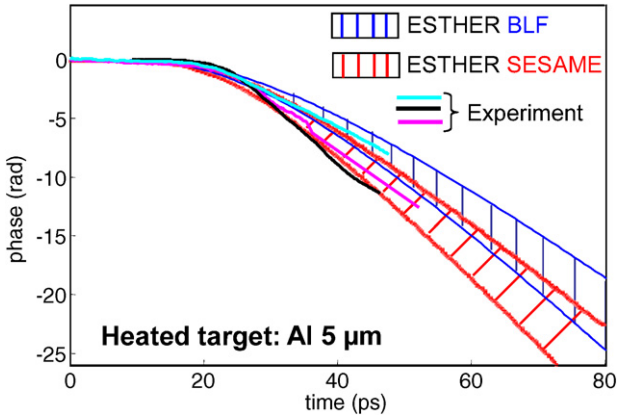

Fig. 9. Experimentally recorded and simulated phases, of the probe beam after reflection from a Al 5 µm thick target, as a function of time.

fluctuations, the SESAME table seems more adequate in modeling the target hydrodynamics in these conditions (solid density, maximum temperature 17 eV).

8. Summary

Laser driven acceleration of ions has opened new perspectives for major applications in scientific, technological (and, potentially, in medical) areas. By directing a high power ultra-short laser pulse onto a thin target, it is now possible to produce beams of high-energy ions and protons, extremely laminar, ultra-short and that can be refocused and energy selected. We have shown the unique interest in using already at present these ion sources: (i) as probing tools for the investigation of high-intensity laser–plasma interactions and quantitative retrieval of electric and magnetic fields in plasmas; and (ii) for isochoric heating of solids. Fast-paced recent progress, both experimental and theoretical [50], indicate routes for further optimization of the ion beams parameters, including the production of ultra-high energy ions (GeV and beyond). This will offer new opportunities for future, unique applications such as radiography of dense matter, injectors, medical applications, ion beam physics, spallation, or transmutation.

References

[1] M. Borghesi, et al., Fusion Sci. Technol. 49 (2006) 412.
[2] M. Borghesi, et al., Phys. Rev. Lett. 92 (2004) 055003.
[3] T. Cowan, et al., Phys. Rev. Lett. 92 (2004) 204801.
[4] B.M. Hegelich, et al., Nature 439 (2006) 441;
M. Hegelich, et al., Phys. Rev. Lett. 89 (2002) 085002;
P. McKenna, et al., Phys. Rev. E 70 (2004) 036405.
[5] H. Schwoerer, et al., Nature 439 (2006) 445.
[6] T. Toncian, et al., Science 312 (2006) 410.
[7] P. Patel, et al., Phys. Rev. Lett. 91 (2003) 125004.
[8] A. Mackinnon, et al., Rev. Sci. Instrum. 75 (2004) 3531.
[9] M. Roth, et al., Phys. Rev. Lett. 86 (2001) 436.
[10] M. Tabak, et al., Phys. Plasmas 1 (1994) 1626.
[11] H. Azechi, et al., Plasma Phys. Controlled Fusion 48 (2006) B267;
M. Dunne, Nat. Phys. 2 (2006) 2.
[12] A. Boyer, et al., Phys. Today 55 (9) (2002) 34.
[13] S.V. Bulanov, et al., Phys. Lett. A 299 (2002) 240.
[14] E. Fourkal, et al., Med. Phys. 29 (2002) 2788.
[15] M. Santala, et al., Appl. Phys. Lett. 78 (2001) 19.
[16] E. Clark, et al., Phys. Rev. Lett. 84 (2000) 670.
[17] R. Snavely, et al., Phys. Rev. Lett. 85 (2000) 2945.
[18] A. Maksimchuk, et al., Phys. Rev. Lett. 84 (2000) 4108.
[19] G. Mourou, T. Tajima, S. Bulanov, Rev. Modern Phys. 78 (2006) 309.
[20] A. Mancic, et al., Rev. Sci. Instrum. 79 (2008) 073301.

[21] N.V. Klassen, L. Zwan, J. Cygler, Med. Phys. 24 (1997) 1924.
[22] S.P. Hatchett, et al., Phys. Plasmas 7 (2000) 2076;
S.C. Wilks, et al., Phys. Plasmas 8 (2001) 542.
[23] K. Nemoto, et al., Appl. Phys. Lett. 78 (2001) 595.
[24] J. Denavit, Phys. Rev. Lett. 69 (1992) 3052–3055;
L. Silva, et al., Phys. Rev. Lett. 92 (2004) 015002;
E. d'Humieres, et al., Phys. Plasmas 12 (2005) 062704.
[25] J. Fuchs, et al., Phys. Rev. Lett. 94 (2005) 045004.
[26] M. Allen, et al., Phys. Rev. Lett. 93 (2004) 265004.
[27] M. Kaluza, et al., Phys. Rev. Lett. 93 (2004) 045003.
[28] T. Ceccotti, et al., Phys. Rev. Lett. 99 (2007) 185002.
[29] S.J. Gitomer, et al., Phys. Fluids 29 (1986) 2679.
[30] P. Mora, Phys. Rev. E 72 (2005) 056401.
[31] L. Romagnani, et al., Phys. Rev. Lett. 95 (2005) 195001.
[32] J. Fuchs, et al., Phys. Rev. Lett. 91 (2003) 255002.
[33] R. Stephens, et al., Phys. Rev. E 69 (2004) 066414.
[34] J.C. Adam, et al., Phys. Rev. Lett. 97 (2006) 205006.
[35] E. Brambrink, et al., Laser Particle Beams 24 (2006) 163–168.
[36] D. Carroll, et al., Phys. Rev. E 76 (2007) 065401, (R).
[37] P. Antici, et al., Phys. Rev. Lett. 101 (2008) 105004.
[38] J. Fuchs, et al., Nat. Phys. 2 (2006) 48.
[39] M. Roth, et al., Phys. Rev. ST-AB 5 (2002) 061002.
[40] H. Ruhl, T. Cowan, J. Fuchs, Phys. Plasmas 11 (2004) L17.
[41] E. Fourkal, et al., Med. Phys. 30 (2003) 1660.
[42] M. Schollmeier, et al., Phys. Rev. Lett. 101 (2008) 055004.
[43] T. Esirkepov, et al., Phys. Rev. Lett. 92 (2004) 175003.
[44] P. Antici, et al., Phys. Plasmas 14 (2007) 030701.
[45] P. Antici, et al., IEEE Trans. Plasma Sci. 36 (2008) 1817.
[46] J. Psikal, et al., Phys. Plasmas 15 (2008) 053102.
[47] S. Buffechoux, et al., submitted for publication (2009).
[48] P. Antici, et al., J. Phys. IV France 133 (2006) 1077.
[49] J.P. Colombier, et al., Phys. Rev. B 71 (2006) 165406.
[50] A. Macchi, et al., C. R. Physique 10 (2) (2009) 207.